Journal of Oceanography, Vol. 63, pp. 1021 to 1028, 2007

Short Contribution

Synoptic Distributions of Thermal Surface Mixed Layer and Thermocline in the Southern Yellow and East China Seas

SUNGHYEA PARK* and PETER C. CHU

Department of Oceanography, Naval Postgraduate School, Monterey, CA 93943, U.S.A.

(Received 8 February 2007; in revised form 16 June 2007; accepted 12 July 2007)

Synoptic distributions of thermal surface mixed layer and thermocline were identified using four airborne expendable bathythermograph (AXBT) surveys (September 1992 and February, May, and September 1993) in the southern Yellow and East China Seas. Seasonality and a dominant driving mechanism of the surface mixed layer were examined. The dominant driving mechanisms differ between seasons and between on-shelf and off-shelf regimes. Currents, eddies, and migration of bottom cold waters (on the shelf) also affect the surface mixed layer. Thermocline thickness, temperature difference from thermocline top to bottom, and thermocline intensity in warm seasons were measured, and their synoptic features were also discussed.

Keywords:
· Yellow/East China Seas,
· thermal surface mixed layer,
· thermocline.

1. Introduction

Four airborne expendable bathythermograph (AXBT) surveys with horizontal spacing of 35 km and vertical resolution of 1 m from the surface to 400 m depth were conducted over the southern Yellow and East China Seas (YES) on 18–29 September 1992 (named as 9209), 4–14 February 1993 (9302), 5–14 May 1993 (9305), and 2–10 September 1993 (9309) (Fig. 1(a)). These data show a variety of synoptic thermal features including the Kuroshio path and intrusion onto the East China Sea (ECS) shelf, thermal frontal structures, finestructures, and cross-frontal heat flux (Furey and Bower, 2005; Park and Chu, 2007a, b). Spatial distributions of thermal surface mixed layer (SML) in 9209 and 9302 and possible causes for these distributions were studied (Furey and Bower, 2005). Taking a closer look at these data, vertical layers, such as thermocline and bottom layer as well as SML, vary seasonally to a great extent (e.g. Fig. 1(b)). Climatological distribution of these vertical layers in the Yellow Sea (YS) derived from the Master Oceanographic Observational Data Set also shows strong seasonality in SML thickness and thermocline temperature jump (temperature difference from thermocline top to bottom) (Chu *et al*., 1997a). The global climatology of SML, however, is unsuitable to represent mesoscale (10–100 km) features revealed by Furey and Bower (2005) because of its low spatial resolution (e.g. $2° \times 2°$ (de Boyer Montégut *et al*., 2004)).

For these reasons, we have studied synoptic characteristics of vertical layers in YES in extension to the work of Furey and Bower (2005). First, we identify the vertical layers from these AXBT data (Section 2) and examine a dominant mechanism for developing SML with supplementary descriptions of seasonality of SML, which are not mentioned by Furey and Bower (2005) (Sections 3 and 4). Second, we explore the characteristics of the thermocline (Section 5). The distributions of the vertical layers in a given year would be a complement to the climatological version of these distributions (e.g. Chu *et al*. (1997a) for YS) or any global datasets (e.g. Kara *et al*. (2003) and de Boyer Montégut *et al*. (2004)) and would be useful for studies such as heat budget, ocean model validation, and primary production dynamics.

2. Vertical Layer Identification

SML is a layer of vertically-uniform temperature, salinity, and density, where active air-sea fluxes generate turbulence to mix the water downward to the SML depth (SMLD), which is the depth of transition from a homogeneous upper layer (i.e. SML) to a stratified layer of the pycnocline (Sprintall and Cronin, 2001). SMLD determined from a temperature profile is not always the same

* Corresponding author. E-mail: spark@nps.edu

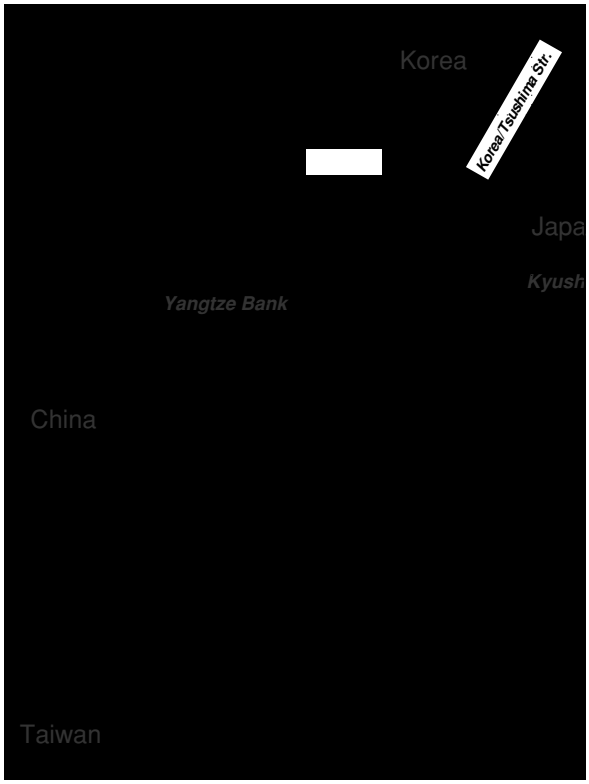

as SMLD determined from a density profile, owing to the salinity effect. In particular, increasing freshwater flux in summer caused by river run-off or precipitation tends to form a shallower density SMLD within a deeper temperature SMLD (Chu *et al*., 2002; Zhang *et al*., 2006). A layer between these two layers is referred to as a salinity-stratified barrier layer. For clarification, the temperature SMLD investigated in this study might be different from density SMLD, especially in summer.

For the temperature profiles on the shelf (shallower than 200 m), a three-layer classification, i.e. SML, thermocline, and bottom mixed layer (BML), is appropriate (Fig. 1(b), top panel) although one layer disappears seasonally in some shelf regions. Off the shelf, profiles reaching 400 m depth (maximum observation depth of the data) display two layers, i.e. SML and thermocline (including seasonal and permanent thermoclines) (Fig. 1(b), bottom panel). Here, the thermocline probably extends deeper than 400 m. Profiles are very sparse at 200–400 m depth, a part of the steep continental slope, and they seldom show BML. Thus, a two-layer classification is appropriate for the region deeper than 200 m.

Two types of criteria, difference and gradient, are commonly used for determining SMLD, as summarized in Chu *et al*. (2002) and Lozovatsky *et al*. (2005, appendix B). The difference criterion requires the deviation of temperature from its surface value to be smaller than a certain fixed value. The gradient criterion requires the vertical gradient of temperature to be smaller than a certain fixed value. We tested both criteria and checked the consistency of SMLDs with the corresponding criteria. Neither criterion was satisfactory for all profiles. The dif-

ference criterion suffers from difficulties in determining wintertime SML in deep regions, i.e. temperature in the upper layer decreases slightly with depth, and is not perfectly isothermal (e.g. 9202 in Fig. 1(b), bottom panel); SML deepens by entrainment at the SML bottom. On the other hand, the gradient criterion is inappropriate when the profiles show vertical fluctuations in small scales within the estimated SML: in these profiles, calculated SMLD is shallower than actual SMLD when judged manually. This difficulty can be overcome if the gradient is measured in a large vertical interval, filtering out the small vertical fluctuations, but not for short profiles on the shelf. Therefore, we use different criteria according to the depth: the difference criterion (0.1°C) for depth <200 m and the gradient criterion (0.025°C/m, mean gradient of the permanent thermocline) elsewhere. The bottom panel in Fig. 1(b) shows the comparison of SMLs obtained using the two criteria. Furey and Bower (2005) applied the same difference criterion as ours to all the profiles, regardless of depth. Since there is no information about the time of the day during the survey, it is assumed that the surveys were conducted in the daytime. The diurnal variation is thus not considered here.

BML is determined by the temperature difference exceeding 0.1°C from the bottom (or at the deepest depth of the profile) upward, the same difference criterion as SML. Accordingly, the thermocline lies between SML and BML. We assume that the thermocline top (bottom) corresponds to SML bottom (BML top). Thermocline thickness (m) is thus defined by vertical distance between thermocline top and bottom. The temperature jump (°C) is defined by the temperature difference between thermocline top and bottom. Thermocline intensity (°C/m) is the mean temperature gradient of thermocline, which is simply defined as the temperature jump divided by thermocline thickness, without consideration of finestructures within the thermocline. If the difference between the two adjacent deepest levels of the profile exceeds 0.1°C (usually on the shelf), BML does not exist.

3. Monin-Obukhov Depth and Depth Ratio

SML is developed generally by wind stirring and convection (i.e. the ocean loses heat), although other mixing mechanisms are also involved, depending on the scale. In order to examine dominant mixing mechanisms for developing SML, the Monin-Obukhov depth

$$L = -\rho C_p u_*^3 \big/ g\alpha\kappa Q \tag{1}$$

is calculated. Here, ρ is the water density; C_p is the specific heat of water at constant pressure; $u_* = \sqrt{\tau/\rho}$ is the friction velocity with the wind stress τ; g is the gravitational acceleration; α is the thermal expansion coefficient; κ(=0.4) is the von Kármán constant; and Q is the surface heat flux (downward positive). The ratio of the surface mixed layer depth D to the Monin-Obukhov depth L

$$\delta = D / L \tag{2}$$

(called depth ratio) determines the SML forcing regimes (Lombardo and Gregg, 1989; Lozovatsky *et al*., 2005): (1) convection regime

$$\delta > 10, \tag{3}$$

(2) wind-forcing regime

$$\delta < 1, \tag{4}$$

and (3) combined forcing regime

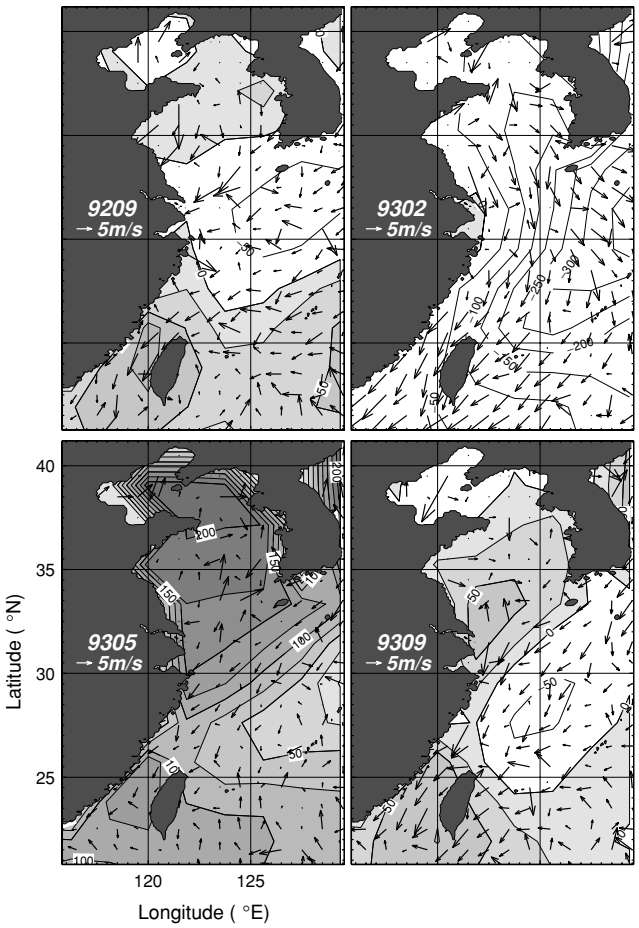

Fig. 2. Net heat flux (W/m^2) and wind speed (m/s) at the sea surface. Contours represent the heat flux and positive values (ocean gains heat) are shaded.

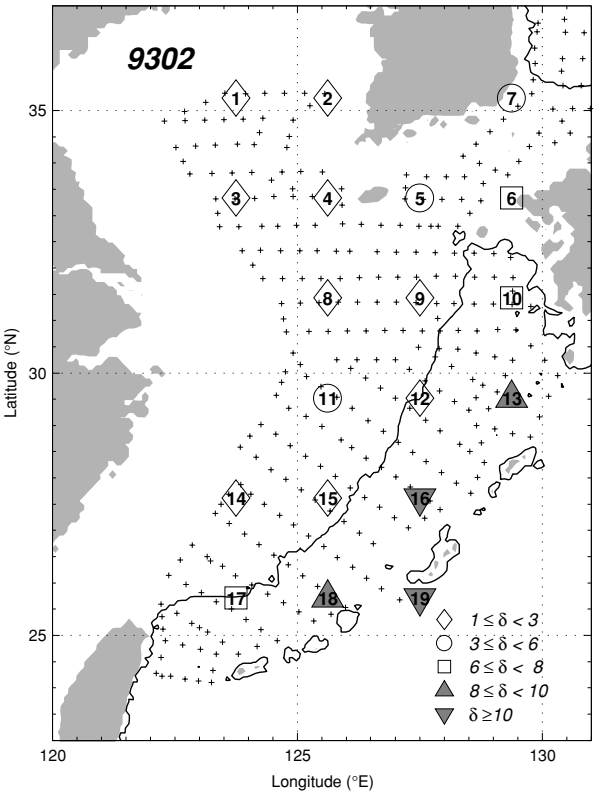

Fig. 3. Depth ratio δ calculated at the grid points of NCEP/NCAR data (in warm seasons the depth ratio is not presented since $\delta < 1$ at most of the points). The values of depth ratios are presented by polygons (refer to the legend at the right bottom of the figure). Numbers in the polygons denote the grid points from G1 to G19 ("G" is omitted in the figure). Small crosses mark locations of AXBT deployments. Thick line marks an isobath 200 m.

$$1 < \delta < 10. \tag{5}$$

We used the monthly National Centers for Environmental Prediction/National Center for Atmospheric Research (NCEP/NCAR) reanalyzed surface flux data (net shortwave radiation, net longwave radiation, latent heat flux, and sensible heat flux) and sea surface temperature data and monthly Coupled Ocean-Atmospheric Data Set (COADS) wind data during the survey period to calculate the Monin-Obukhov depth and to explore atmospheric forcings. These data were obtained from the NOAA-CIRES Climate Diagnostics Center, Boulder, Colorado, USA (see the website at http://www.cdc.noaa.gov). Here, downward heat flux is taken as positive (Fig. 2). The depth ratio is calculated at the grid points of the NCEP/NCAR data (T62 Gaussian grid, i.e. 1.87° × 1.90° of longitude × latitude), which is coarser than the COADS data (1° × 1°). Figure 3 shows the depth ratio estimates displayed by polygons with numbers G1 to G19 ("G" is omitted in the figure). The wind data are noisy in the Bohai Sea (north of 37°N) and near the land-sea boundary. However, these noisy wind data were not used for the calculation because they are outside the coverage of the AXBT data.

4. Surface Mixed Layer

4.1 September (9209 and 9309)

SML in the southern YS and the northern Yangtze Bank (YB) is deeper in 9209 (<40 m) than in 9309 (<20 m), owing to stronger wind and larger negative heat flux (Figs. 2 and 4). In September surveys (9209 and 9309), the heat flux has both signs (upward or downward), but the depth ratio is $\delta < 1$ in all the regions (not shown here), indicating that the wind mixing dominates over the convective mixing.

When the Kuroshio Front shifts seaward more in 9309 than in 9209 (Furey and Bower, 2005), the Yellow Sea Bottom Cold Water (YSBCW) and the modified YSBCW migrate further southward, as shown by the 18°C isotherm in Fig. 4 (see also Park and Chu (2007b, figure 3)) and the vertical temperature sections along isobaths 80–100 m spanning from the southern YS trough to the Yangtze Bank: the bottom cold waters migrate along these isobaths (Fig. 5). The shallow SML with a thickness <20 m extends consistently to the southern boundary of those bottom cold waters, ~30.5°N (~31.5°N) in 9309 (9209) (Figs. 4 and 5). The SML deepens abruptly crossing the boundary of the bottom cold waters (Stn-10–Stn-12 in Fig. 5-9209; Stn-11–Stn-12 in Fig. 5-9309). Vertical temperature fluctuations formed from below a strong upper thermocline to a thermocline bottom (dotted lines in Fig. 5) disappear when crossing the boundary of the bottom cold waters. Based on these features, the bottom cold waters on the shallow (<100 m) shelf change stratification and eventually impede SML deepening by wind. On the other hand, the southern migration of the Korea Strait Bottom Cold Water (KSBCW) does not shallow the SML as much as YSBCW and modified YSBCW do, since KSBCW exists at depths deeper than 100 m with much smaller thickness (see Park and Chu (2007b, figure 11)).

The thin SML is patchlike along inner/shoreward and outer/seawardsides of the Kuroshio Front (KF), and thick SML lies between the inner and outer KF (see warm (>26°C), thick SML region in 124–126°E and 25–27°N (9209) and along a line from (123.5°E, 25.5°N) to (128°E, 30°N) (9309)). In 9209 the thick patch (>60 m) in 128–130°E and 29–32°N is related to a warm eddy induced by meandering of the eastern branch of the Kuroshio: in 127–128°E and 29–30°N the Kuroshio is divided into the eastern branch, which flows eastward south of Kyushu and eventually exits through the Tokara Strait, and the north-

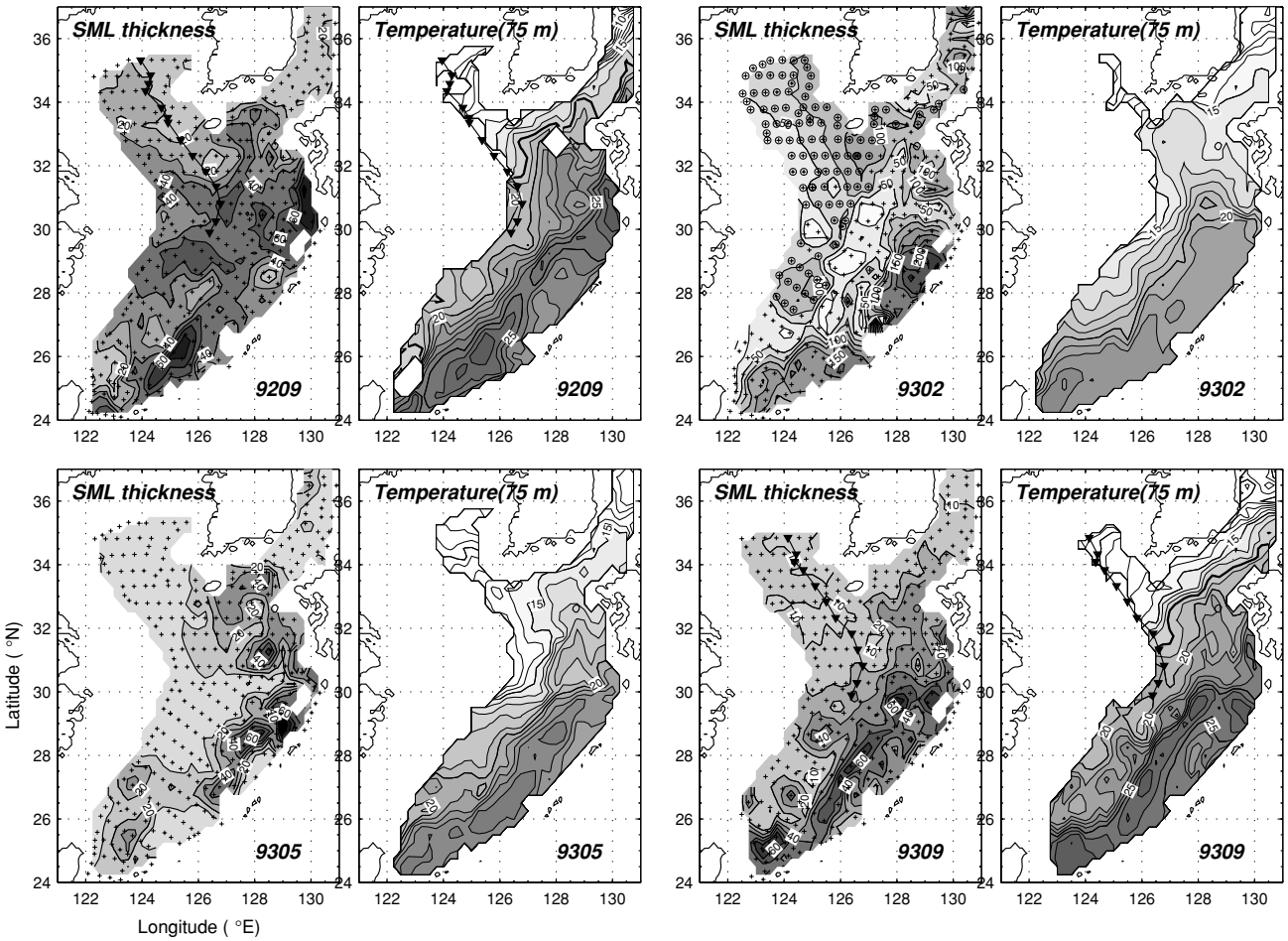

Fig. 4. Surface mixed layer thickness and temperature at 75 m depth. Note that contour interval of the surface mixed layer thickness is 25 m in 9302 and 10 m elsewhere. Contour interval of isotherms is 1°C and isotherms are labeled every 5°C. An 18°C isotherm is thickened in 9209 and 9309. Small crosses mark locations of AXBT deployments, and large open circles do where the surface mixed layer extends to the bottom. Curved lines with triangles are locations in Fig. 5.

ern branch (i.e. the Tsushima Warm Current; see further explanation in Subsection 4.2). It is also thick in the other surveys despite its displacement. In 9209 the thin SML (<20 m) off northeast Taiwan is related to a cold water dome on the shelf (see Furey and Bower (2005, figure 5)).

4.2 February (9302)

On the shelf shallower than 100 m SML is fully developed from the surface to the bottom (see circles in Fig. 4-9302 and Furey and Bower (2005, figure 2b)), and the depth ratio is $1 < \delta < 3$ (G1–G4, G8, G14 in Fig. 3) indicating the combined regime; however, the wind mixing is stronger than the convective mixing. Along thermal fronts, especially KF, the depth ratio is small, $1 < \delta < 3$ (G9, G12, G15 in Fig. 3), despite a strong heat loss of around –300 W/m^2. This is due to the shallow (<50 m) SML along thermal fronts, especially KF (see the good agreement of shallow SML and large horizontal thermal gradient in Fig. 4-9302 and Furey and Bower (2005, figure 2b)). This shallow SML zone with a width around 100 km is maintained by the local balance between weakening winds and strong vertical temperature/density gradient in the front (Ivanov *et al*., 2004; Furey and Bower, 2005, figure 3a).

Away from this shallow SML zone, the situation is reversed. The depth ratio is $\delta > 8$ beyond the seaward side of KF (see grey-colored triangles in the region roughly deeper than 200 m in Fig. 3), indicating the dominance of convective mixing over wind mixing. Here, SML is thickest: it is thicker than the value estimated by Furey and Bower (2005). This thick, warm SML implies that in addition to the convective mixing, downward advection of the warm water also contributes to the SML deepening.

The depth ratio is $\delta \sim 5$ in G5 and G7 and $\delta \sim 6$ in

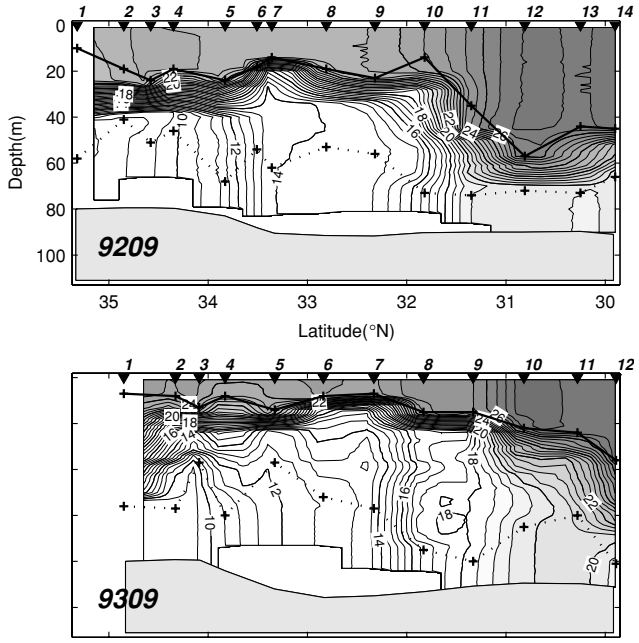

Fig. 5. Vertical temperature section along isobaths 80–100 m spanning from the southern Yellow Sea trough to the Yangtze Bank (see the curved lines with triangles in Fig. 4 for the locations). The triangles with numbers on the top of the figure, which correspond to the triangles in Fig. 4, denote stations of AXBT deployments, numbered from the north (Stn-1–Stn-14 for 9209; Stn-1–Stn-12 for 9309). Bottom cold waters reside against strong upper thermoclines. The estimated surface (bottom) mixed layer is marked by a solid (dotted) line with crosses.

G6, indicating the combined regime. In this region, a large amount of heat escapes from the ocean supplied by the Tsushima Warm Current, which branches from the Kuroshio at 127–128°E and 29–30°N, flows northward, turns east around Cheju Island, and then flows toward the Korea/Tsushima Strait (Huh, 1982; Lie *et al*., 1998; Hsueh, 2000; Furey and Bower, 2005). In G9 and G12, located along the Tsushima Warm Current upstream, heat loss is also large, but the depth ratio is $\delta \sim 1$. The difference of depth ratios between the two regions seems to be related to differences in the winds and/or the stratification in the two regions along the current.

4.3 May (9305)

Since the heat flux is downward for all regions and the depth ratio is $\delta < 1$ (not shown), the wind mixing dominates SML. The increasing downward heat flux in the spring erodes the previous winter's thick SML from the surface, yielding a new SML. The new SML, however, hardly deepens because of the weak wind in 9305 and is therefore the thinnest SML in the four surveys (<10 m on the shelf) (9305 in Figs. 2 and 4). Two thick SML regions near (123.5°E, 27°N) and (123.5°E, 25°N) are related to warm eddies caused by meandering or intrusion of the Kuroshio. Variation of thick, patchlike SML on the shelf deeper than 100 m north of 30°N seems to be induced by the Tsushima Warm Current. These SML features imply that in regions influenced by strong currents, especially in warm seasons, SML is locally modified by currents.

5. Thermocline

5.1 Thermocline thickness

In warm seasons the horizontal distributions of thermocline thickness resemble the bathymetry (Fig. 6(a)), as presented in the Yellow Sea (Chu *et al*., 1997a). This is because the thermocline thickness is generally proportional to the ocean depth where the ocean depth is shallower than the typical depth of the thermocline bottom; the permanent thermocline is located typically at 400–1000 m depth in the subtropics (Java Ocean Atlas at http://odf.ucsd.edu/joa/jsindex.html). Indeed, the thermocline thickness is thinnest (<20 m) over YB, where the depth is the shallowest among the AXBT deployment stations. However, the thickness changes locally in each survey from the southern part of the YS trough (123–124.5°E, 34–35.5°N) and south of Cheju Island (125–127°E, 29–33°N) to the shelf from south of YB to Taiwan.

In the southern part of the YS trough (123–124.5°E and 34–35.5°N), the thermocline is thin (20–30 m) in 9209 due to thick SML and YSBCW, but thick (30–50 m) in 9309 due to weak winds. In 9305 the thermocline is even thicker (from 40 up to 60 m) than both September surveys, because increased positive heat flux with weak winds in May shallows the SML. South of Cheju Island the thermocline is thicker (40–80 m) in September surveys than in the May survey (<40 m). This thick thermocline is due to the development of thermocline intrusions in the lower part of the thermocline, which is represented by multiple inversions (i.e. multilayered structures) of temperature profiles at the thermocline depth and induced by vertically sheared advection between cold, fresh shelf water and warm, salty Kuroshio-oriented water (Lee *et al*., 2003; Park and Chu, 2007a, b). From south of YB to Taiwan the thermocline on the shelf is thin in 9209 when the Kuroshio axis is located shoreward than its canonical path, whereas it is thick in 9309 following the canonical path (Furey and Bower, 2005). In addition, it is modified by the Kuroshio intrusion, Kuroshio meandering, and Taiwan Warm Current variation.

5.2 Thermocline temperature jump and intensity

As YES continues to be heated through September based on the annual variation of the heat flux (Hirose *et*

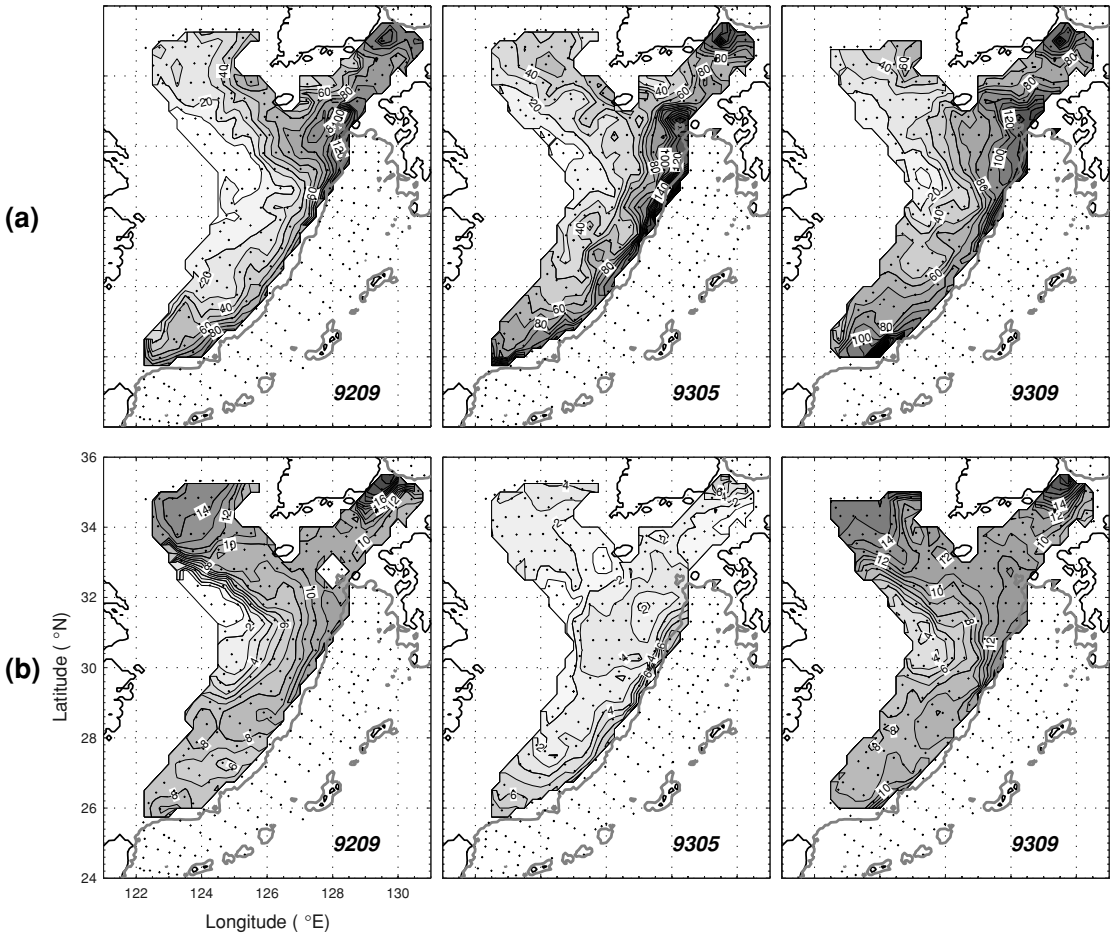

Fig. 6. (a) Thermocline thickness (m), (b) thermocline temperature jump from its bottom to top (°C). Small crosses mark locations of AXBT deployments. Thick grey line marks an isobath 200 m.

al., 1999; Chu *et al*., 2005), the thermocline reaches its greatest depth in September during the year (Chu *et al*., 1997a, b). For this reason, the thermocline temperature jump in September generally resembles the bathymetry (9209 and 9309 in Fig. 6(b)). On the shallowest shelf (i.e. YB), the thermocline thickness and temperature jump are minimum (Figs. 6(a) and (b)) owing to not only the shallow depth but also strong bottom tidal mixing (Lee and Beardsley, 1999), which might erode the bottom of the thermocline. The temperature jump increases from YB (2–4°C) toward the shelfbreak (10–12°C); however, the thermocline intensity is almost constant (0.1–0.2°C/m) because the thermocline thickness increases simultaneously. Above YSBCW both temperature jump (12–14°C) and thermocline intensity (0.4–0.8°C/m) are large, whereas above the Korea Strait Bottom Cold Water the jump is large (12–20°C) but the intensity is weak because of a thick, irregularly-shaped thermocline (Park and Chu, 2007a).

As heat flux in YS (ECS) changes its sign from negative in February (April) to positive in March (May), the water column warms. Temperature at 10 m depth increases 2–4°C from 9302 in most regions, and the warming extends to greater depth (not shown). May, however, is an early stage of the warming, so the thermocline is not fully developed. As a result, the thickness in 9305 is comparable to September surveys, but the temperature jump is <4°C in most regions, unlike September surveys (9305 in Figs. 6(a) and (b)).

6. Conclusions

We have identified the surface mixed layer and the thermocline using the four AXBT surveys in the southern Yellow Sea and the East China Sea and explored their seasonality and plausible causes. The depth ratio, δ, i.e. the ratio of the surface mixed layer depth to the Monin-Obukhov depth, was estimated for diagnosing the dominant driving mechanism of the surface mixed layer: convection regime for $\delta > 10$; wind-forcing regime for $\delta < 1$; and combined forcing regime for $1 < \delta < 10$.

In September the surface mixed layer is about 30 m deep over the continental shelf and is driven by wind mixing (rather than convective mixing): $\delta < 1$. As the shallow surface mixed layer with thickness <~20 m extends consistently from the Yellow Sea trough to the southern boundary of the Yellow Sea Bottom Cold Water and the modified Yellow Sea Bottom Cold Water on the shelf, those bottom cold waters impede the surface mixed layer deepening by wind mixing. The surface mixed layer shows patchiness along the Kuroshio Front due to the Kuroshio meandering. Regardless of seasons, it is shallower, along the axis of the Kuroshio Front than away from the axis, but its detailed features vary with seasons. In February, strong convective mixing dominates the surface mixed layer deepening beyond the seaward side of the Kuroshio Front ($\delta > 8$), and wind stirring dominates the surface mixed layer deepening on the continental shelf ($1 < \delta < 3$). In the Tsushima Warm Current region the depth ratio is different upstream (δ~5) and downstream (δ~1), which seems to be related to difference in the winds and/or the stratification in the two regions along the current. In May the surface mixed layer is shallowest (<10 m on the shelf), owing to weak wind and evident surface heating throughout the regions: $\delta < 1$. Currents, meandering, and eddies also influence the surface mixed layer locally.

The thermocline thickness in May is comparable to that in September, but temperature jump is much smaller (<4°C) in May due to immaturity of the thermocline. Overall horizontal distributions of the thermocline thickness in warm seasons resemble the bathymetry, but there are local changes from the southern part of the Yellow Sea trough and south of Cheju Island to the shelf between south of the Yangtze Bank and Taiwan. In September the temperature jump (12–14°C) and the thermocline intensity (0.4–0.8°C/m) are large above the Yellow Sea Bottom Cold Water. On the other hand, the temperature jump (12–20°C) is large, but the thermocline intensity (0.1–0.3°C/m) is weak above the Korea Strait Bottom Cold Water because of the thick irregular-shaped thermocline.

Acknowledgements

This research was sponsored by the Naval Oceanographic Office, Office of Naval Research, and Naval Postgraduate School.

References

Chu, P. C., C. R. Fralick, S. D. Haeger and M. J. Carron (1997a): A parametric model for Yellow Sea thermal variability. *J. Geophys. Res.*, **102**(C5), 10499–10508.

Chu, P. C., S. K. Wells, S. D. Haeger, C. Szczechowski and M. Carron (1997b): Temporal and spatial scales of the Yellow Sea thermal variability. *J. Geophys. Res.*, **102**(C3), 5655–5668.

Chu, P. C., Q. Y. Liu, Y. L. Jia and C. W. Fan (2002): Evidence of barrier layer in the Sulu and Celebes Seas. *J. Phys. Oceanogr.*, **32**, 3299–3309.

Chu, P. C., Y. C. Chen and A. Kuninaka (2005): Seasonal variability of the East China/Yellow Sea surface buoyancy flux and thermohaline structure. *Adv. Atmos. Sci.*, **22**, 1–20.

de Boyer Montégut, C., G. Madec, A. S. Fischer, A. Lazar and D. Iudicone (2004): Mixed layer depth over the global ocean: An examination of profile data and a profile-based climatology. *J. Geophys. Res.*, **109**, C12003, doi:10.1029/2004JC002378.

Furey, H. and A. Bower (2005): The synoptic Temperature Structure of the East China and southeastern Japan/East Seas. *Deep-Sea Res. II*, **52**, 1421–1442.

Hirose, N., H.-C. Lee and J.-H. Yoon (1999): Surface heat flux in the East China Sea and Yellow Sea. *J. Phys. Oceanogr.*, **29**, 401–417.

Hsueh, Y. (2000): The Kuroshio in the East China Sea. *J. Mar. Sys.*, **24**, 131–139.

Huh, O. K. (1982): Spring-season flow of the Tsushima Current and its separation from the Kuroshio: satellite evidence. *J. Geophys. Res.*, **87**, 9687–9693.

Ivanov, A. Y., W. Alpers, K. T. Litovchenko, M. He, Q. Feng, M. Fang and X. Yan (2004): Atmospheric front over the East China Sea studied by multisensor satellite and in situ data. *J. Geophys. Res.*, **109**, C12001, doi:10.1029/2004JC002432.

Kara, A. B., P. A. Rochford and H. E. Hurlburt (2003): Mixed layer depth variability over the global ocean. *J. Geophys. Res.*, **108**(C3), 3079, doi:10.1029/2000JC000736.

Lee, J.-H., H.-J. Lie and C.-H. Cho (2003): The structure of ocean fronts in the East China Sea. *Proceedings of the 12th PAMS/JECSS Workshop*, Hangzhou, China, 2-10-1~2.

Lee, S.-H. and R. C. Beardsley (1999): Influence of stratification on residual tidal currents in the Yellow Sea. *J. Geophys. Res.*, **104**(C7), 15679–15701.

Lie, H.-J., C.-H. Cho and J.-H. Lee (1998): Separation of the Kuroshio water and its penetration onto the continental shelf west of Kyushu. *J. Geophys. Res.*, **103**, 2963–2976.

Lombardo, C. P. and M. C. Gregg (1989): Similarity scaling of viscous and thermal dissipation in a convecting surface boundary layer. *J. Geophys. Res.*, **94**, 6273–6284.

Lozovatsky, I., M. Figueroa, E. Roget, H. J. S. Fernando and S. Shapovalov (2005): Observations and scaling of the upper mixed layer in the North Atlantic. *J. Geophys. Res.*, **110**, C05013, doi:10.1029/2004JC002708.

Park, S. and P. C. Chu (2007a): Characteristics of thermal finestructures in the southern Yellow and East China Seas from airborne expendable bathythermograph measurements. *J. Oceanogr.* (submitted).

Park, S. and P. C. Chu (2007b): Thermal fronts and cross-frontal heat flux in the southern Yellow Sea and East China Sea. *Acta Oceanologica Sinica* (submitted).

Sprintall, J. and M. F. Cronin (2001): Upper ocean vertical structure. p. 3120–3129. In *Encyclopedia of Ocean Sciences*, Vol. 6, ed. by J. Steele, S. Thorpe and K. Turekian, Academic Press, London, U.K.

Zhang, Y., D. Wu and X. Lin (2006): The barrier layer in the East China Sea in summer. *EOS Trans. AGU*, Western Pacific Geophys. Meet. Supp., Abstract OS11B-0101.